

Supporting information

Revealing Degradation Mechanisms in 3D/2D

Perovskite Solar Cells under Photothermal

Accelerated Ageing

Zijian Peng^{1,9}, Andrej Vincze³, Fabian Streller⁴, Vincent M. Le Corre^{1,2}, Kaicheng Zhang¹, Chaohui Li^{1,9}, Jingjing Tian^{1,9}, Chao Liu^{1,2}, Junsheng Luo^{1,6}, Yicheng Zhao^{1,6}, Andreas Späth^{4,5}, Rainer Fink⁴, Thomas Heumüller^{1,2}, Andres Osvet¹, Ning Li^{1,2,7}, Martin Stolterfoht⁸, Larry Lüer¹, Christoph J. Brabec^{1,2}

¹Institute of Materials for Electronics and Energy Technology (i-MEET), Friedrich-Alexander-Universität Erlangen-Nürnberg, 91058 Erlangen, Germany

²Helmholtz-Institute Erlangen-Nürnberg (HI ERN), 91058 Erlangen, Germany

³International Laser Centre SCSTI, 84104 Bratislava, Slovak Republic

⁴Chair of Physical Chemistry II, Friedrich-Alexander-Universität Erlangen-Nürnberg, 91058 Erlangen, Germany

⁵Competence Center Engineering of Advanced Materials, Friedrich-Alexander-Universität Erlangen-Nürnberg, 91058 Erlangen, Germany

⁶National Key Laboratory of Electronic Thin Films and Integrated Devices, School of Integrated Circuit Science and Engineering, University of Electronic Science and Technology of China (UESTC), 611731 Chengdu, P. R. China

⁷State Key Laboratory of Luminescent Materials and Devices, Institute of Polymer Optoelectronic Materials and Devices, School of Materials Science and Engineering, South China University of Technology, 510640 Guangzhou, P. R. China

⁸Electronic Engineering Department, The Chinese University of Hong Kong, Hong Kong SAR, China

⁹Graduate School in Advanced Optical Technologies (SAOT), 91052 Erlangen, Germany

Email: zijian.peng@fau.de, larry.lueer@fau.de, christoph.brabec@fau.de

Methods

Materials

FAI, MABr, BAI, OAI, PEA_I, PEABr, PEASCN, BDAI₂, CF₃PMAI, CF₃PAI EDAI₂ and PDAI₂ were bought from Greatcell Solar Materials. PbI₂, PbBr₂, CsI were purchased from Sigma-Aldrich. FPEAI, Tris(pentafluorophenyl)borane (BCF), HDAI₂, ODAI₂, DMe-PDAI₂ and DMe-EDAI₂ were purchased from TCI. PCBM was purchased from Nano-C. Poly[2,2'''-bis[(2-butyl octyl)oxy]carbonyl]-[2,2':5',2":5",2'''-quaterthiophene]-5,5'''-diyl] (PDCBT) was purchased from 1-Material. PTAA, GuaiI, CyMAI, Br-PMAI, ThEAI, CyDMAI₂ and PhDMAI₂ was purchased from Xi'an Yuri Solar. The SnO₂ nanoparticle solution was purchased from Alfa Aesar. All the solvents mentioned were purchased from Sigma-Aldrich.

Device fabrication

Perovskite solar cells were prepared according to previous work with some adjustment.¹ ITO substrates were cleaned with oxygen plasma for 5 min. SnO₂ solution was diluted with water (1:5), then spin-coated on the ITO substrates at 3000 rpm 25 s and annealed at 150 °C for 30 min. Before being transfer into N₂ glovebox, SnO₂ substrates were treated with oxygen plasma for 3 min. PCBM solution (10 mg/mL in CB/DCB 9:1) was spin-coated on substrates and annealed at 150 °C for 10 min.

1.5 M stoichiometric perovskite precursors of Cs_{0.05}MA_{0.1}FA_{0.85}PbI_{2.75}Br_{0.25} (CsMAFA) or Cs_{0.15}FA_{0.85}PbI_{2.75}Br_{0.25} (CsFA) were obtained by dissolving salts into DMF:DMSO=4:1 (CsMAFA) or DMF:DMSO:NMP=4:0.5:0.5 solution (CsFA). Precursor was spin-coated at 5000 rpm for 50 s, and the 300 μL anisole was dropped at 25 s. The wet film was annealed at 150 °C 10 min.

Different passivators were dissolved in IPA to achieve desired concentration (such as 10 mM) and dynamically spin-coated onto perovskite and annealed at 100°C for 5 min. For example, once the substrate reached the target spin speed (4000 rpm), 50 µL of the passivation solution was quickly dropped in the middle of the substrate, and then maintained at the target spin speed for 20 seconds. In the case of BDAI₂ passivation, due to its low solubility in IPA/toluene (3-5 mM), after the substrate reached 4000 rpm, first droplet of saturated solution was dropped onto the substrate, wait for 2 s until the solvent evaporated and the substrate was dry again, then the second droplet of saturated solution was dropped, and keep at 4000 rpm for 20 seconds (e.g., 2-3 times of saturated solution corresponding to 10 mM passivation). In case of target-2D-di bottom sample, BDAI₂ solution (10 mg/mL, in DMF) was spin-coated on ETL and annealed at 100 °C 10 min, before the deposition of perovskite layer.

PDCBT (6 mg/mL in chloroform) and PTAA (15 mg/mL in chlorobenzene with 10 wt% BCF as dopant) were dynamically deposited on perovskite films at 2000 rpm and 4000 rpm for 25 s, respectively. After annealing at 90 °C for 10 min, films were transfer into thermal evaporator and a 40 nm Au layer was evaporated. The active area of 0.06 cm² is defined by the overlap between the mask and the ITO.

2D films deposition

Solution of mono-ammonium spacers and PbI₂ (mol ratio: 2:1), and di-ammonium spacers and PbI₂ (mol ratio: 1:1) were dissolved into DMSO with the concentration of 0.4M at room temperature. After cleaning the glass substrate with ozone-plasma cleaning, 50 µL of solution was dropped onto the glass and spin-coated at 4000 rpm for 30 s. Then samples were annealed at 100°C for 5 min.

J-V measurement

J-V characteristics were measured with a Keithley source measurement unit and a WAVELABS SINUS-70 3A solar simulator, which provides illumination with an AM1.5G spectrum and light intensity of 100 mW cm^{-2} . The *J-V* characteristics were performed from 0 to 1.2 V (forward scan) and from 1.2 to 0 V (backward scan) at a scan rate of 30 ms/step and a scan step of 40 mV. The light intensity was calibrated with a Si reference cell (91150V) bought from Newport.

Operational stability measurement

Devices without encapsulation were loaded into a degradation chamber flowed with N_2 flow. Light source was provided by 4 white LED (XLamp® CMA3090 LED) without using additional filter. The light intensity was controllable and adjusted to 1-sun or 2-sun equivalent intensity by measuring and matching the same or double J_{SC} value of the devices under AM 1.5G solar simulator (e.g. $21\text{-}23 \text{ mA cm}^{-2}$ for 1-sun, $42\text{-}46 \text{ mA cm}^{-2}$ for 2-suns). A hotplate underneath the chamber was set to desired temperature and a temperature sensor (PT100) was installed inside the chamber and put against to one of the device's corner to record the temperature trend. The *J-V* characteristics were measured by LabView program with different interval time (2-10 minutes in the early stages and 45-90 minutes in the later stages). Samples were loaded under either open-circuit or 0.7 V bias during ageing.

Characterization

Work function (WF) was performed with a SPS040 Kelvin Probe from KP Technology. The tip's WF was determined by using a highly oriented pyrolytic graphite (HOPG) with a WF ~ 4.6 eV. Photoluminescence and absorption spectra were carried out by Tecan Infinite 200 PRO. X-ray diffraction (XRD) patterns were taken from a Panalytical X'pert powder diffractometer with filtered Cu K α radiation ($\lambda = 1.54178 \text{ \AA}$) and an X'Celerator solid-state stripe detector.

The impedance spectra were measured by Zahner Zennium Pro potentiostat, under short-circuit and different illumination controlled by LED lamp (LSW-2, s/n LS 1858).

X-ray photoelectron spectroscopy (XPS) was performed on an EA 125X U7 Energy Analyser from Scienta Omicron using Al K-alpha radiation with 1486.7 eV excitation energy, 0.05 eV step and 20 eV pass energy.

The Time-of-flight secondary ion mass spectrometry (ToF-SIMS) depth profiles were acquired by using a Time-of-Flight SIMS IV (Ion-TOF GmbH, Muenster, Germany) equipped with a Bi⁺ primary ion gun working at 25 keV in dual beam mode. The sputtering was realized with 2 keV O₂ source (for positive ions) and 1 keV Cs source (for negative ions) using of active electron flooding to prevent the surface charging to increase the yield of positively and negatively charged secondary ions.

Numerical simulation

Optical simulation was done with Setfos software. Drift diffusion was done with SIMsalabim tool developed by Koster et al. (<http://simsalabim-online.com>).² The simulation parameters are listed in Table S 3.

pK_a calculation

The pK_a value is calculated using the pK_a calculators from Chemaxon.

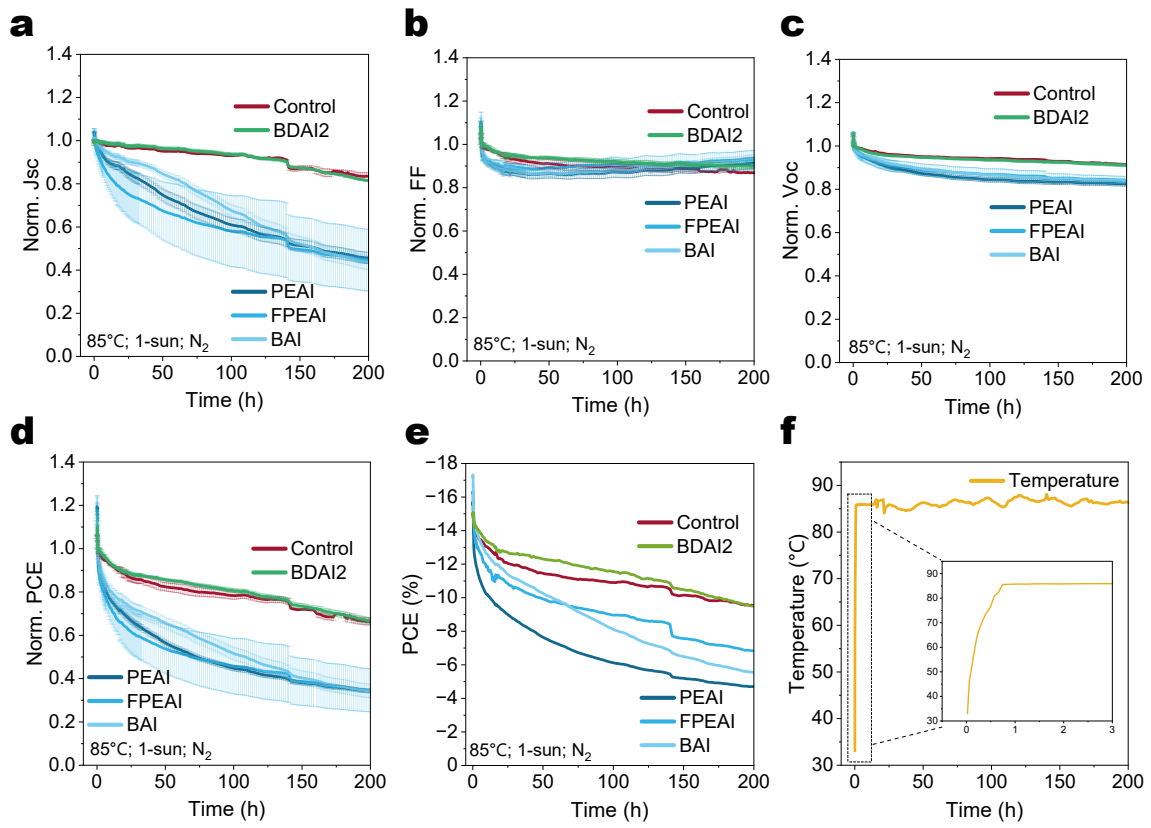


Figure S 1 The operational stability of 3D/2D-mono-ammonium and 3D/2D-di-ammonium based passivated perovskite solar cells under 85 °C and 1-sun condition. (a-d) Those parameters were obtained from the J - V curves during degradation and normalized by the value at 0.6 hour. Each type of cell contains three individual cells and the error bars represent the standard deviation. (e) The unnormalized PCE of devices. Each color represents one individual device. (f) The recorded temperature during the stability measurement. The sharp drop of PCE at the very beginning (0 - 0.6 h) is due to the of negative temperature coefficient from around 30°C to 85°C. The small stepwise drop of PCE and J_{SC} around 140 h is due to the fluctuation of the light source.

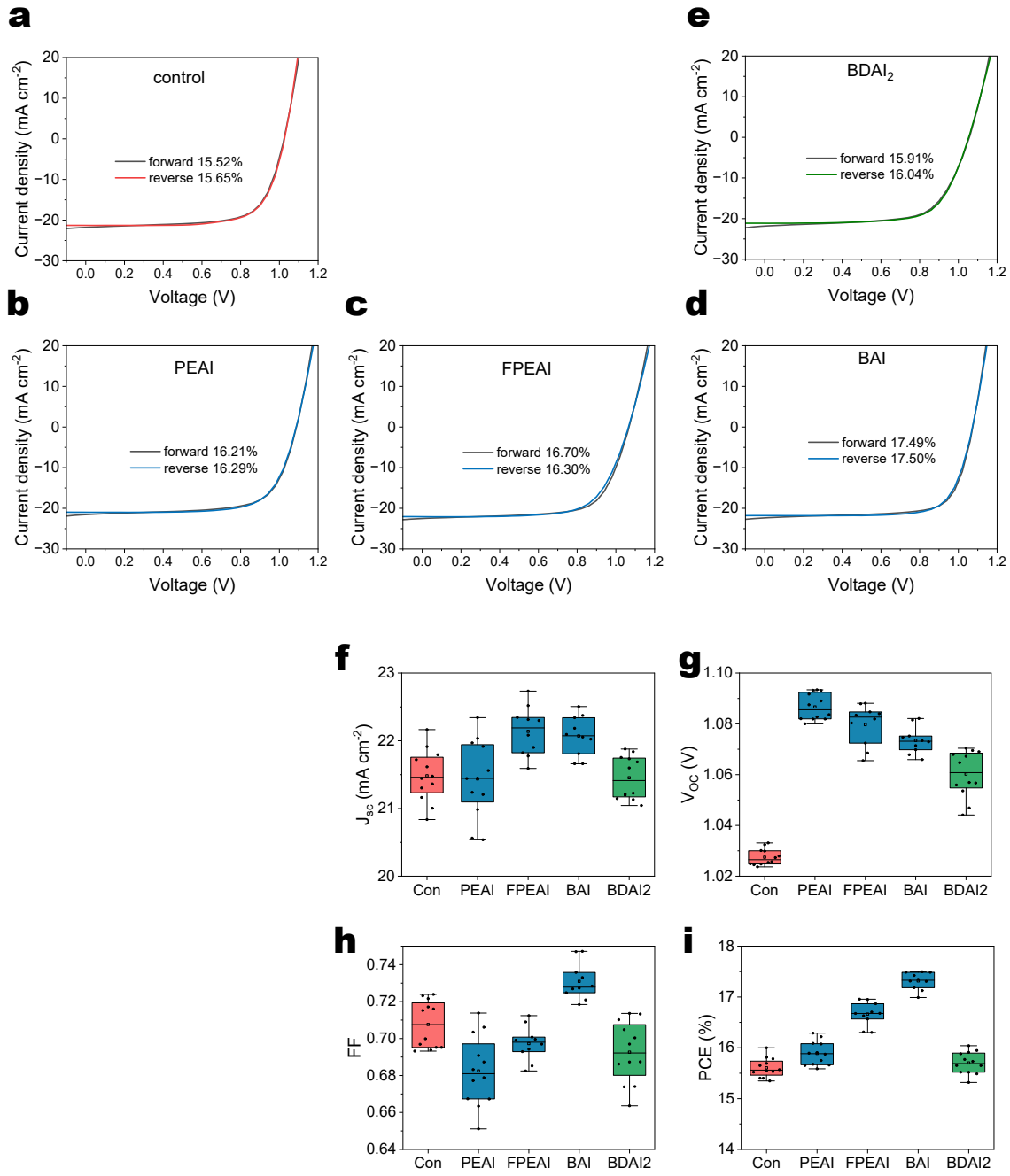


Figure S 2 (a-e) The forward and reverse J - V curves and (f-i) statistical results of device parameters for 3D/2D-mono-ammonium and 3D/2D-di-ammonium based devices.

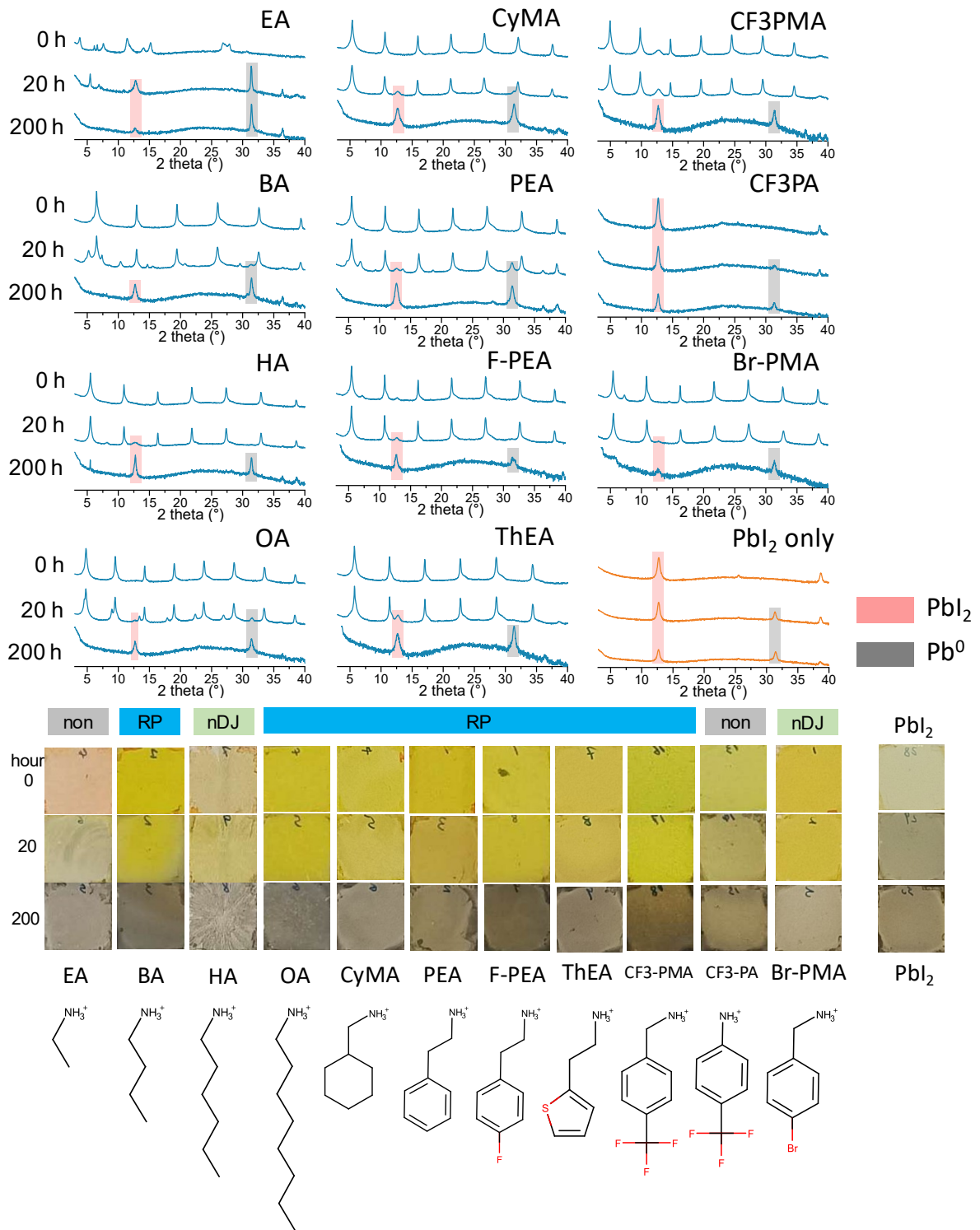


Figure S 3 Upper part: XRD patterns of different films formed by 2 mol mono-cation iodide and 1 mol PbI₂ (2 AI + 1 PbI₂) before and after ageing at 85 °C and 2-suns. Lower part: the corresponding phase (RP, near-DJ (nDJ) and no 2D phase forming (non)) together with the photograph. EA³ and CF₃PA are labelled as “non”, since their mixture with PbI₂ do not have corresponding characteristic diffraction peak along (100) planes in XRD patterns. HA and Br-PMA are labelled as “nDJ”, since their offsets of inorganic layers are small and hence have near-DJ stacking^{4,5}.

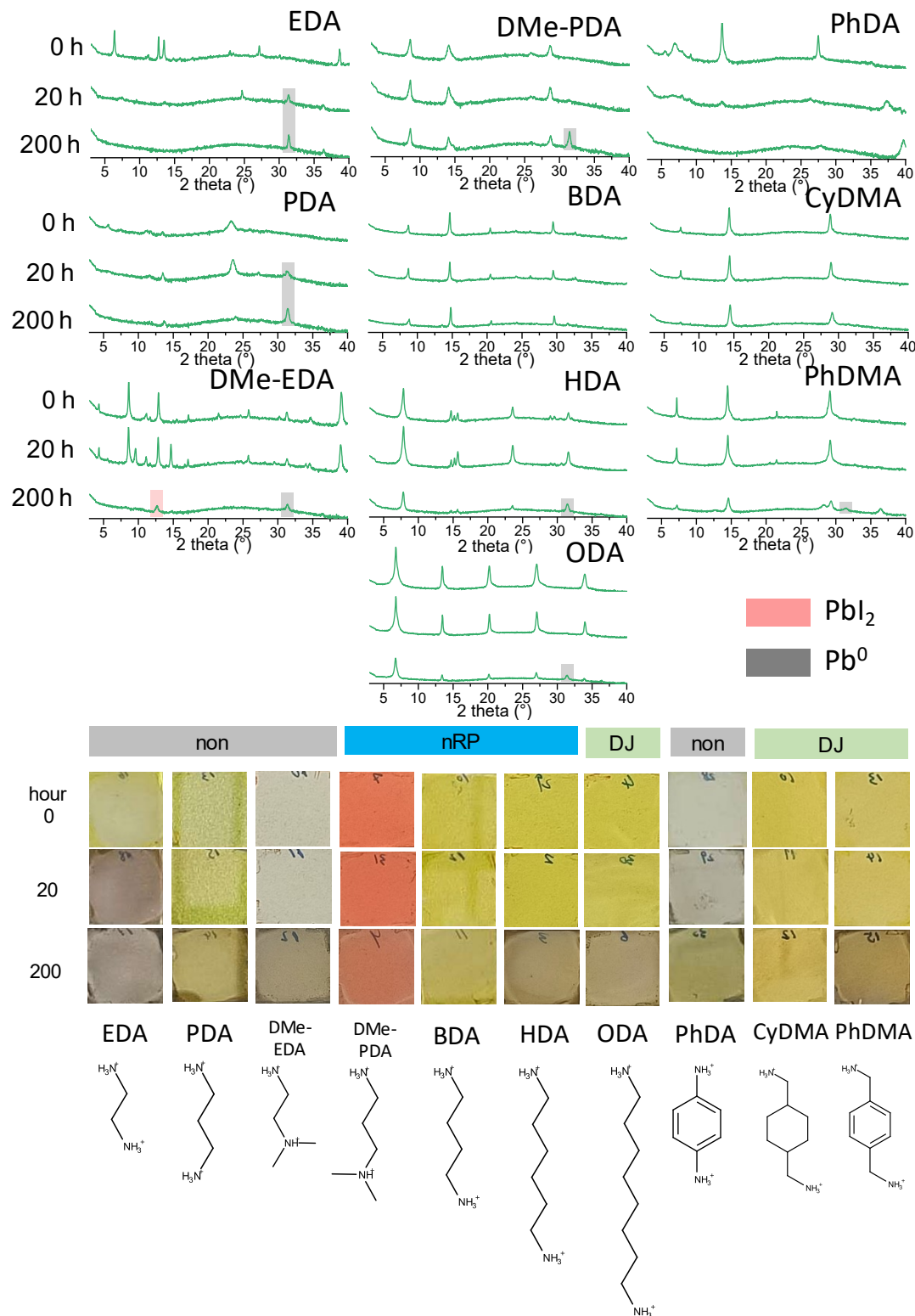


Figure S 4 Upper part: XRD patterns of different films formed by 1 mol di-cation iodide and 1 mol PbI_2 ($\text{Al}_2 + \text{PbI}_2$) before and after ageing at 85 °C and 2-suns. Lower part shows the corresponding phase (DJ, near-RP (nRP) and no 2D phase forming (non)) together with the photograph. EDA, PDA⁶, DMe-EDA and PhDA^{7,8} are labelled as “non”, as they do not have 2D (100) planes in XRD patterns. DMe-PDA, BDA and HDA are labelled as “nRJ”, since their offsets of inorganic layers are large and hence have near-RP stacking^{6, 9-11}.

Table S 1 The summary of the photo-thermal stability (85°C and 2-suns) of organic-inorganic compounds formed by different spacers and PbI₂. Those, whose XRD patterns change largely or Pb⁰ peak emerge after 200 hours or color change obviously, are labelled as “unstable”. Here both RP (nRP) and DJ (nDJ) refer to the n=1 case.

	RP or nRP	DJ or nDJ	non-2D
mono-ammonium	unstable	unstable	unstable
di-ammonium	relatively stable	relatively stable	unstable

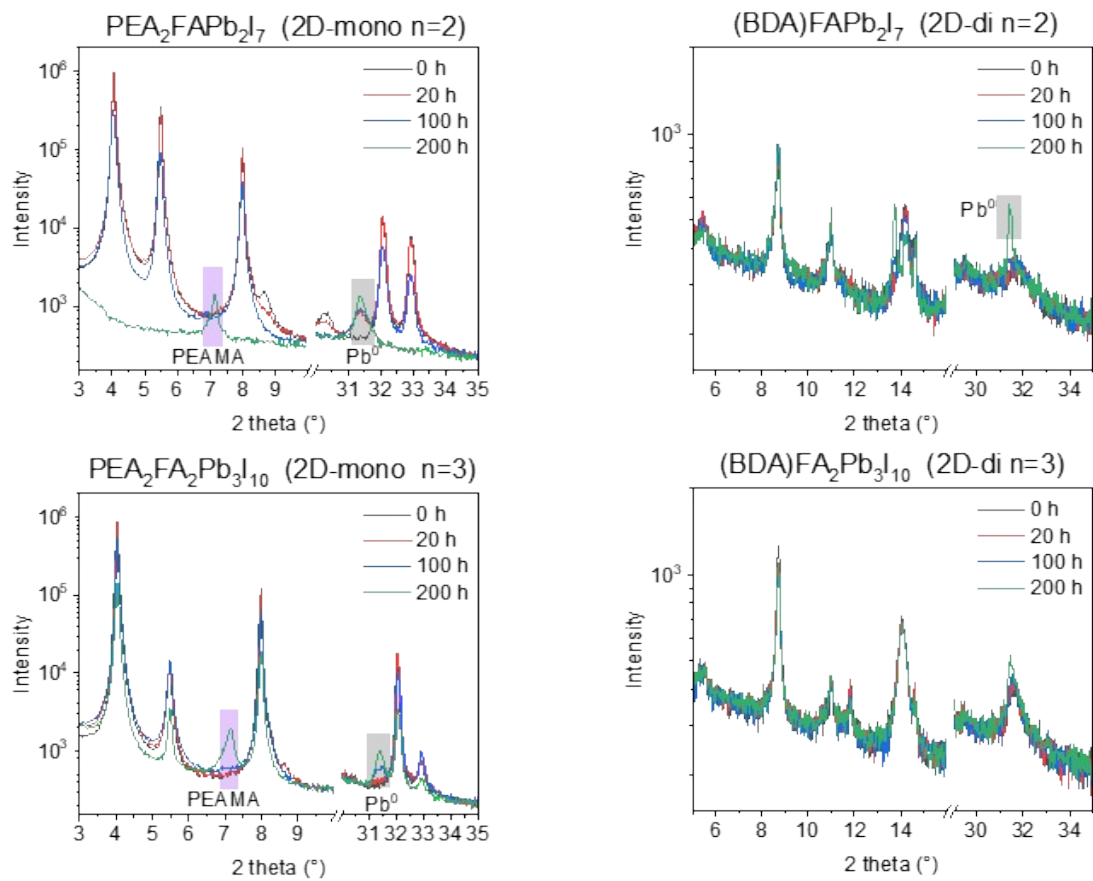


Figure S 5 The XRD patterns of 2D-mono-ammonium and 2D-di-ammonium perovskite (n=2 and 3) before and after ageing at 85 °C and 2-suns. For PEA based 2D, the diffraction peak emerged at around 7° can be attributed to the product of (phenethylamino)methaniminium (PEAMA^+), suggesting the reaction between PEA and FA¹².

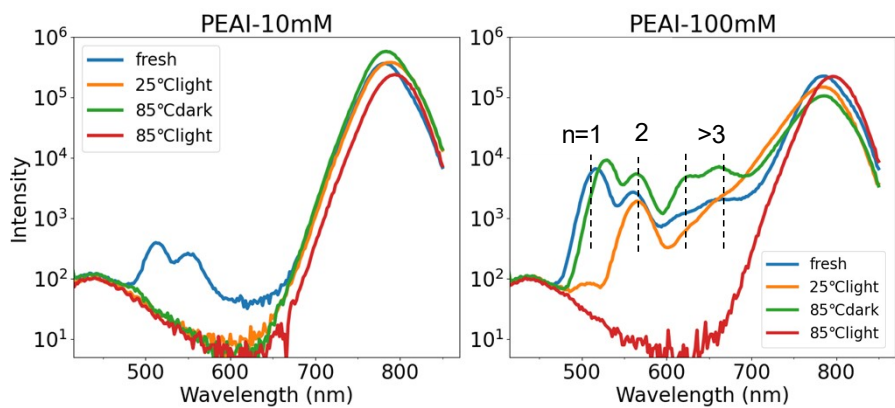


Figure S 6 The PL spectra of PEAI passivator (with 10 mM and 100 mM concentration) on 3D perovskite after ageing at different conditions for 300 hours. The wide peak at 450 nm is due to the fluorescence of the glass substrate itself.

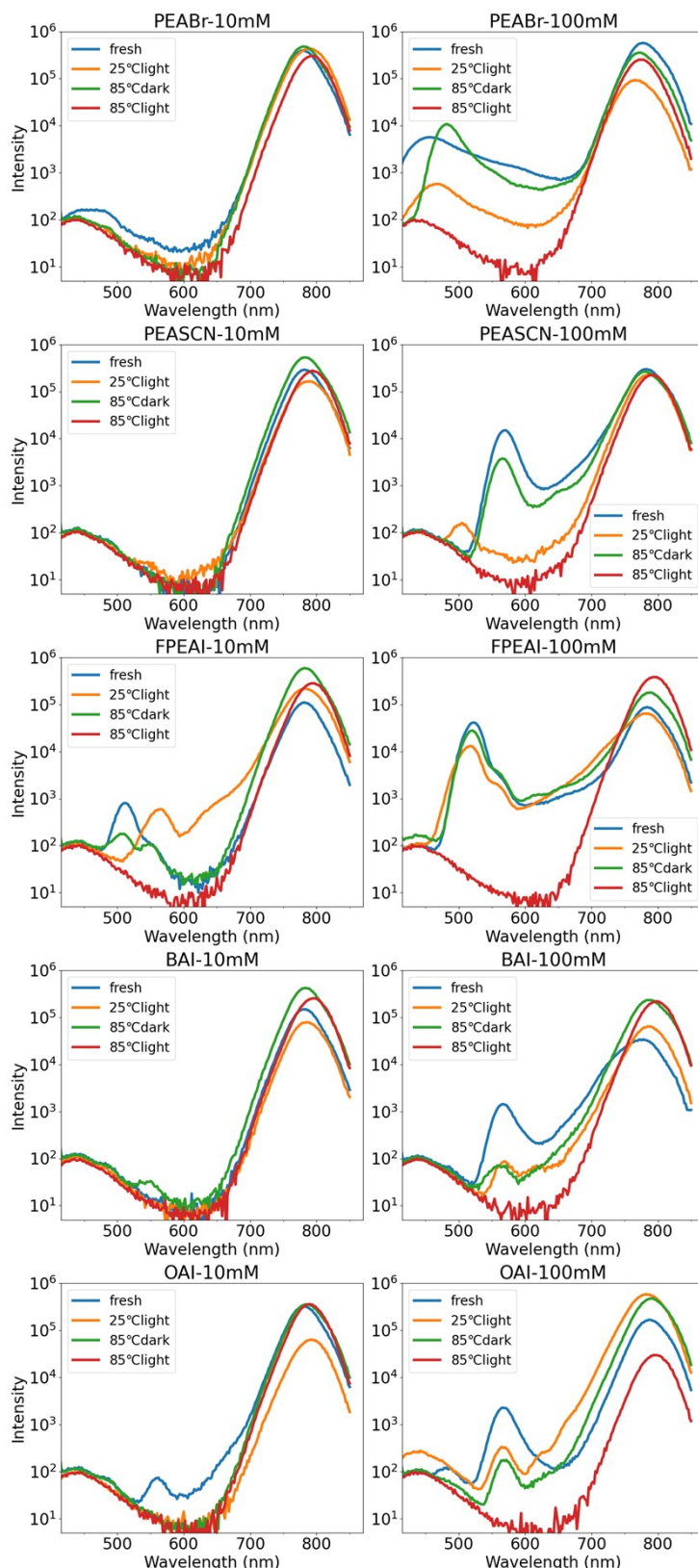


Figure S 7 PL spectra of 3D perovskite films with different concentration of mono-ammonium passivators after ageing at light, heat, and light-heat conditions for 300 hours. The wide peak at 450 nm results from the fluorescence of the glass substrate itself.

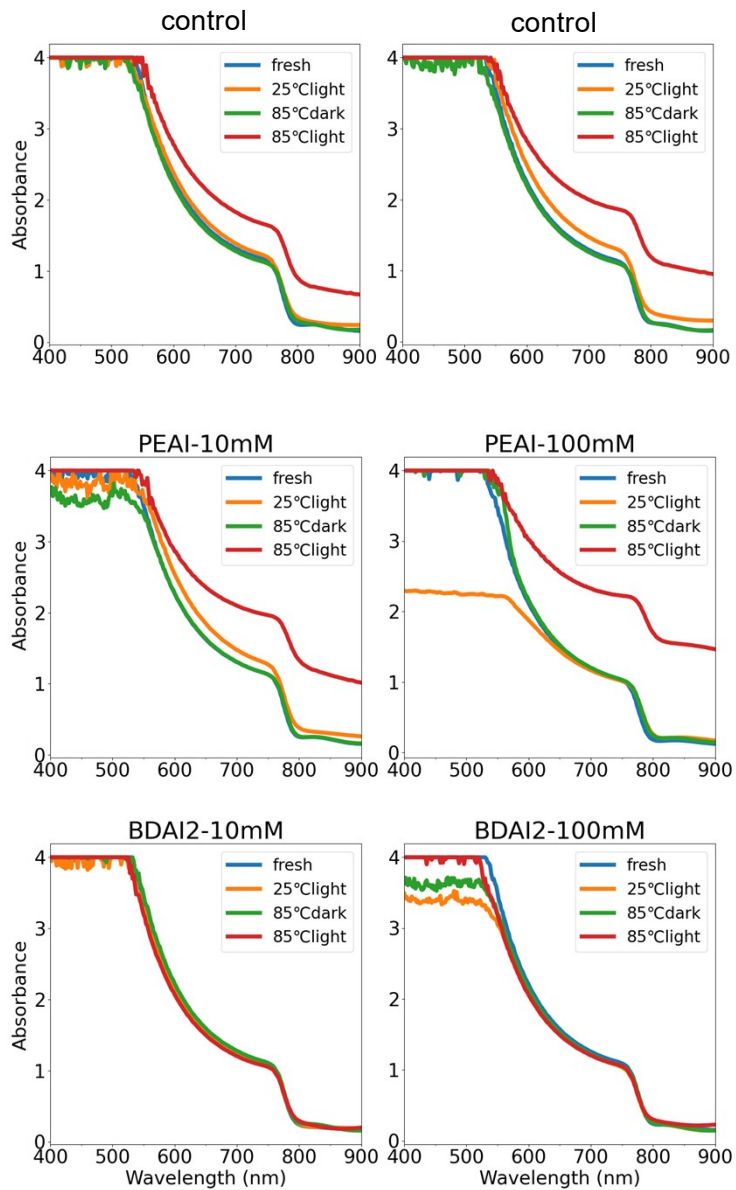


Figure S 8 UV-Vis spectra of 3D perovskite films with different concentration of passivators after ageing at light, heat, and light-heat conditions for 300 hours.

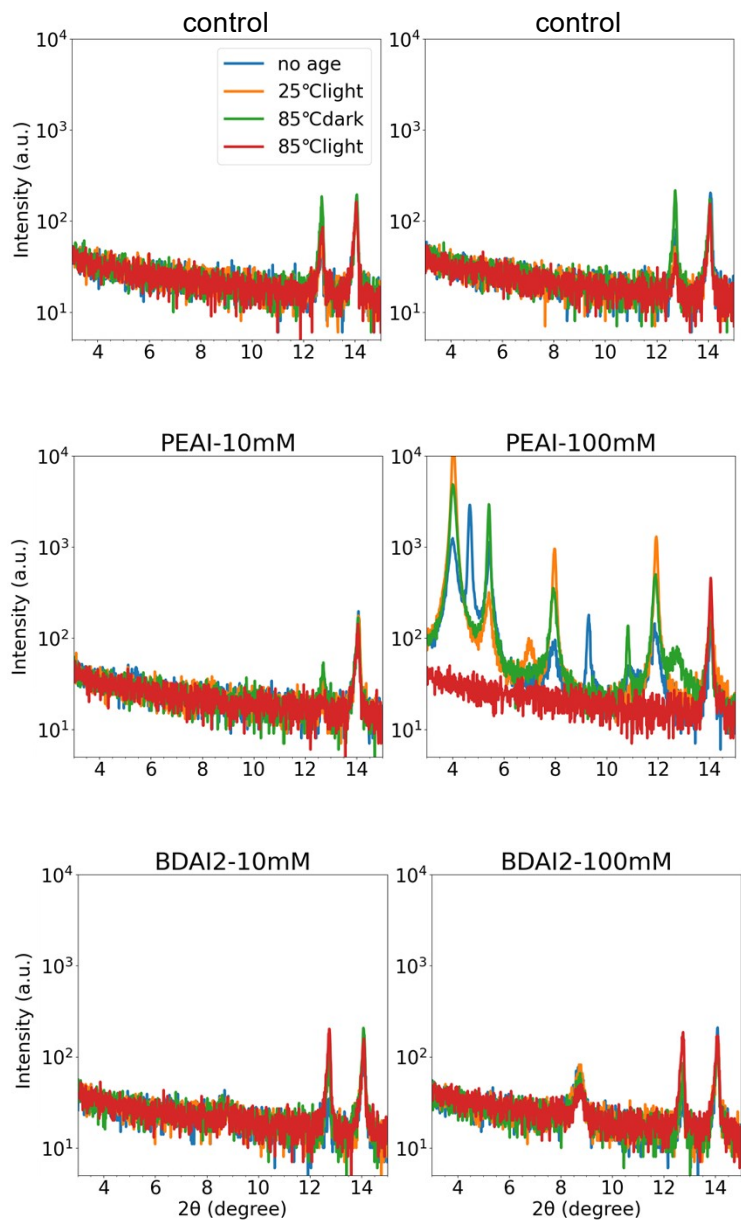


Figure S 9 XRD patterns of 3D perovskite films with different concentration of passivators after ageing at light, heat, and light-heat conditions for 300 hours.

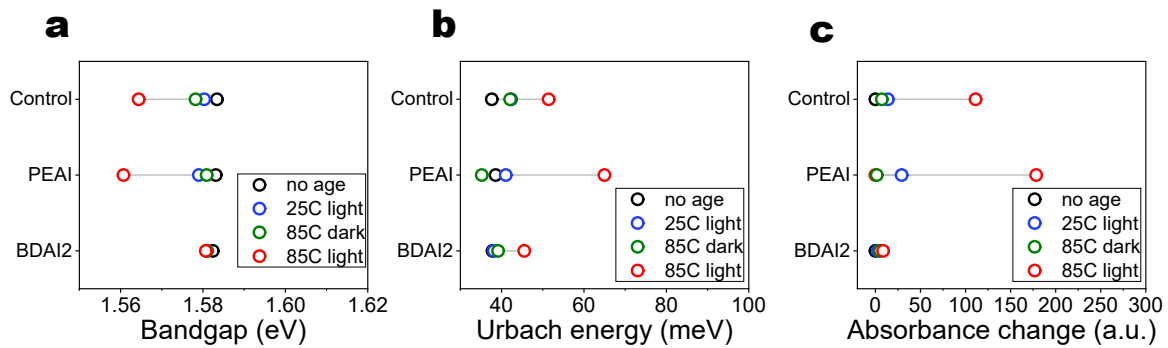


Figure S 10 (a) Bandgap, (b) Urbach energy and (c) absorbance change (area integration between fresh and aged samples at 650-850 nm region) are calculated from UV-Vis data (Figure S 8). Concentration of 10 mM was shown here. The combination of light and heat has great influence on 3D perovskite.

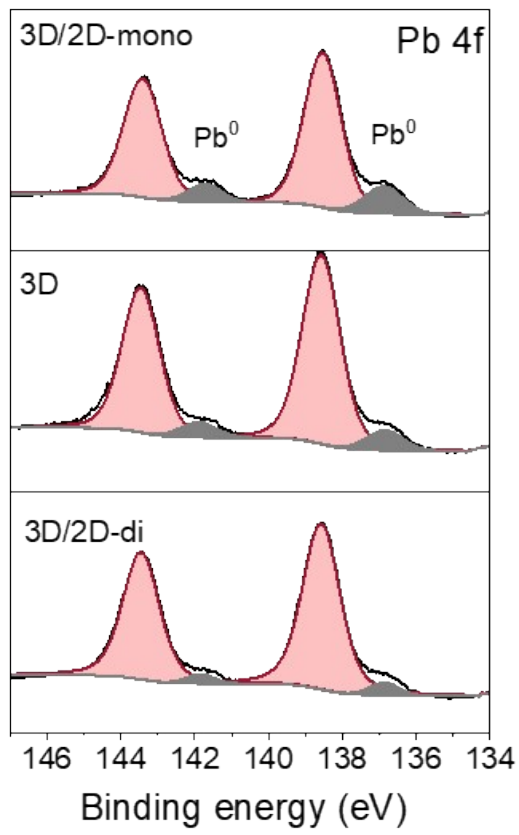


Figure S 11 XPS spectra of 3D, 3D/2D-mono and 3D/2D-di devices after 300 h ageing at 85 °C 2-suns. The perovskite films were exposed by removing the gold electrode with scotch tape, and washing upper transport layers away with chlorobenzene.

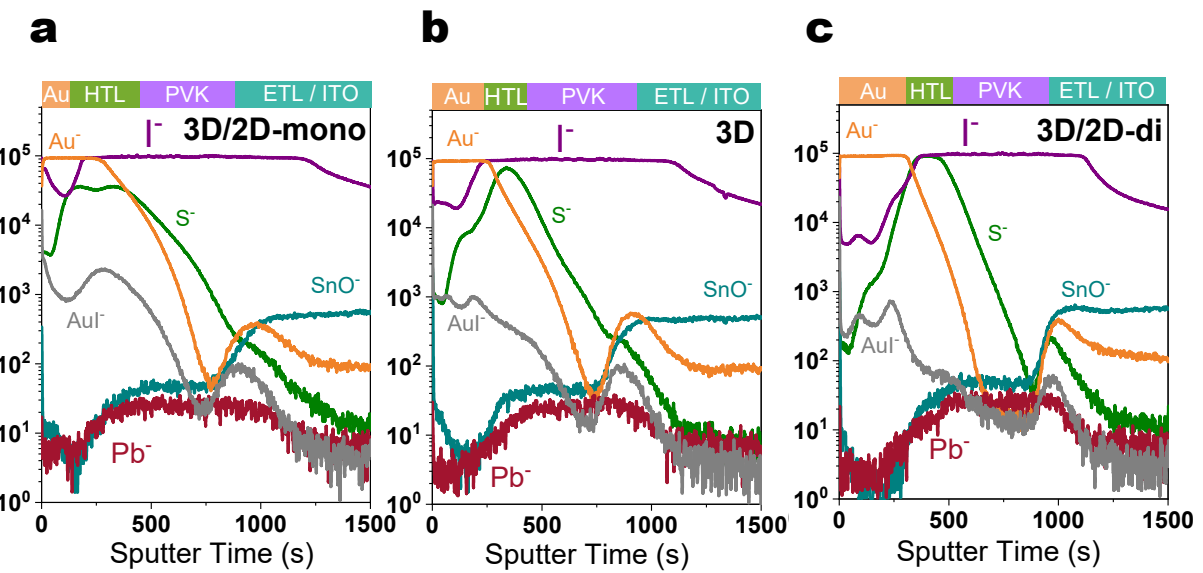


Figure S 12 ToF-SIMS depth profiles of the aged 3D/2D-mono, 3D and 3D/2D-di devices (300 hours under 85 °C 2-suns).

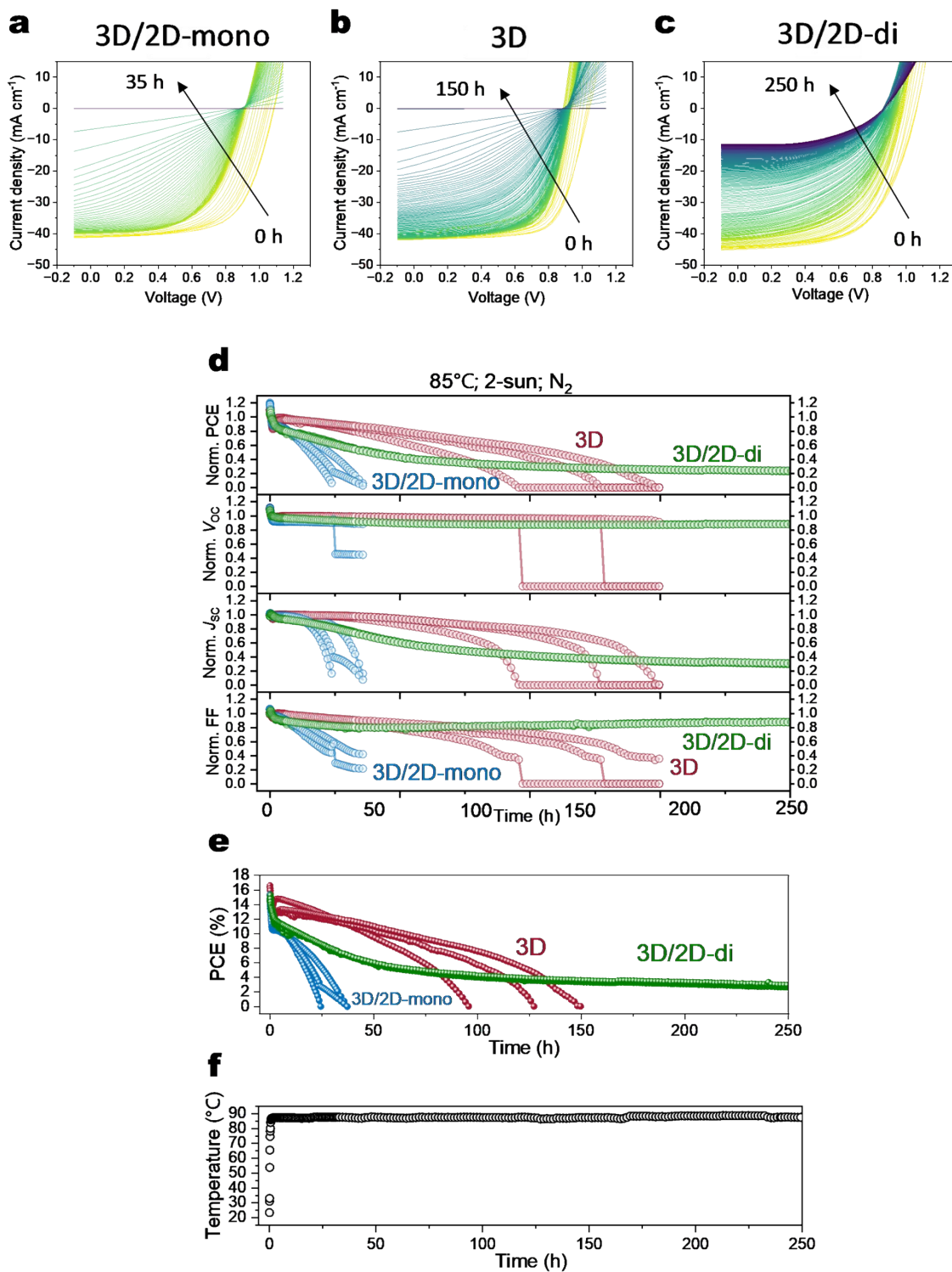


Figure S 13 Operational stability under 85°C and 2-suns illumination. (a-c) Reverse J - V curves of 3D/2D-mono, 3D and 3D/2D-di devices at different ageing time. (d) The normalized parameters dependent on time. Each color contains 3 independent devices. (e) The unnormalized PCE dependent on time. Each color contains 3 individual devices. As there is a fast burn-in at the very beginning due to the negative temperature coefficient, data were normalized at 0.6 h when the chamber's temperature increased to $80\text{-}85^{\circ}\text{C}$ (f).

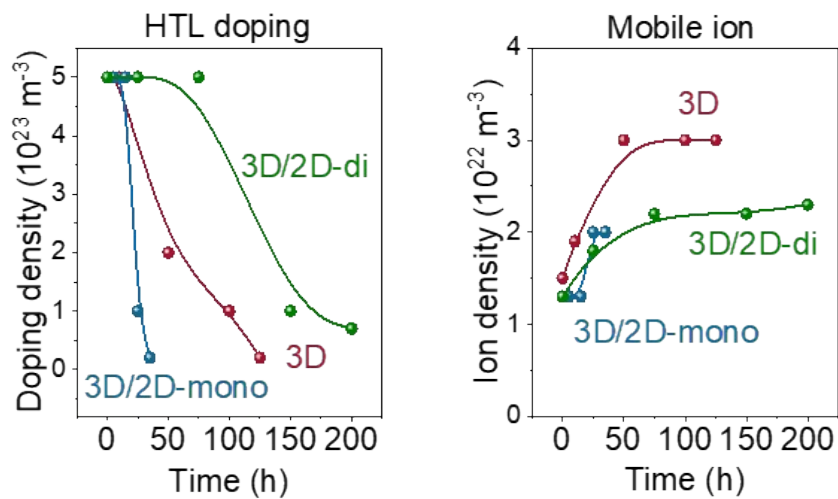


Figure S 14 Corresponding simulation parameters (HTL doping concentration and mobile ion density) obtained at various ageing time.

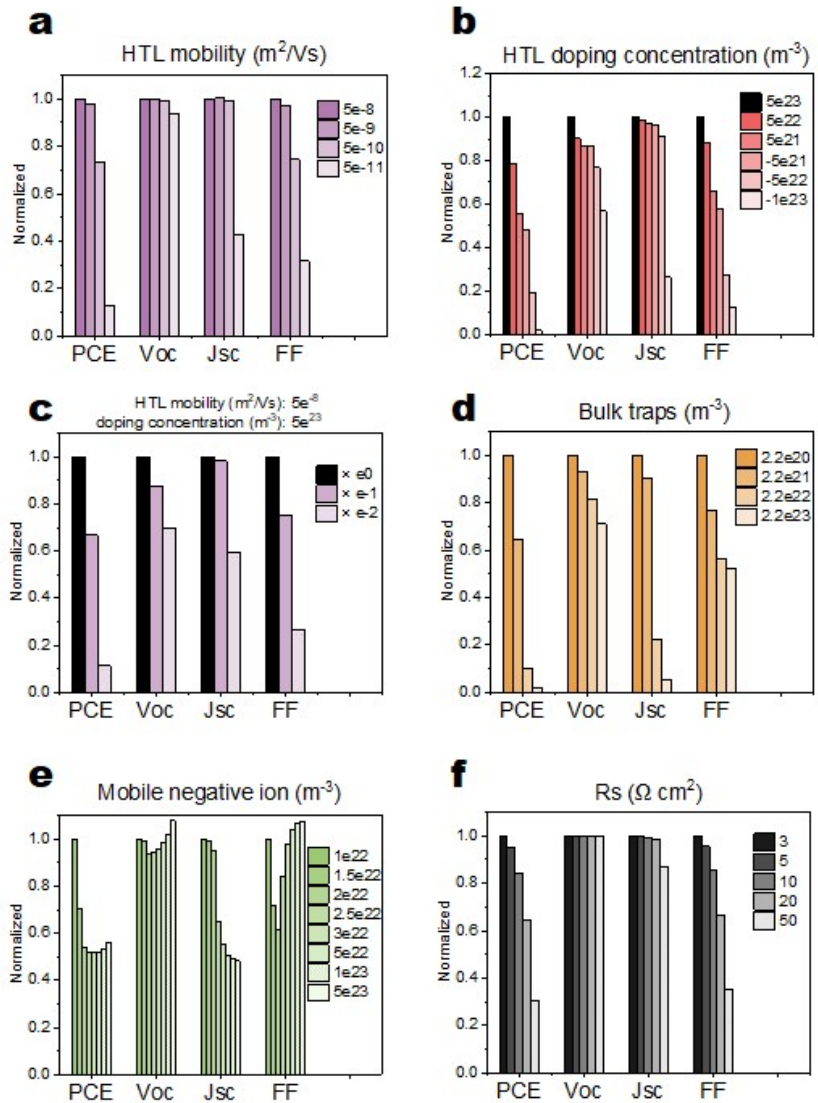


Figure S 15 Trends in PCE, V_{OC} , J_{SC} and FF with different simulation parameters. It shows how $J-V$ parameters (PCE, V_{OC} , J_{SC} and FF) change by only changing one or two simulation parameters at one time. The $J-V$ parameters are normalized by the initial values (3D sample at 0.6 h under 85°C and 2-suns). For example, in case of the first graph (HTL mobility), it shows that the FF loss dominates when it decreases the HTL mobility from 5×10^{-8} to $5 \times 10^{-11} \text{ m}^2/\text{Vs}$. In case of HTL doping concentration, when the legends change from $5\text{e}23$ to $-1\text{e}23 \text{ m}^{-3}$ (from p to n type), FF loss dominates the PCE losses as well. For bulk trap density, both J_{SC} and FF losses are primary losses as the bulk trap density increases from $2.2\text{e}20$ to $2.2\text{e}23 \text{ m}^{-3}$.

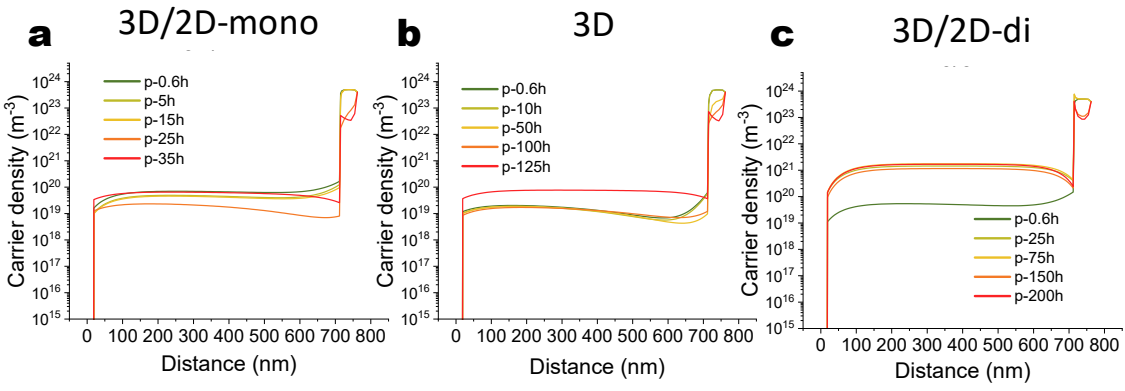


Figure S 16 Carrier (hole) diagram from the simulation result.

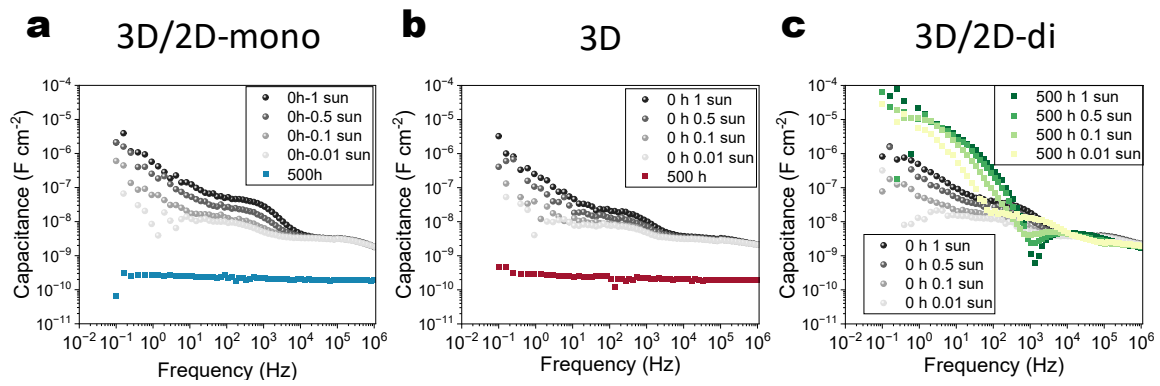


Figure S 17 Capacitance versus frequency plot of samples before and after 85 °C 2-suns degradation. The impedance was carried out at short-circuit and different illumination intensities. The aged 3D and 3D/2D-mono devices exhibit high resistance and lack of frequency-dependent capacitance. The aged 3D/2D-di has 2 order of magnitude increased of low frequency response, which is likely attributed to the increased recombination rate¹³.

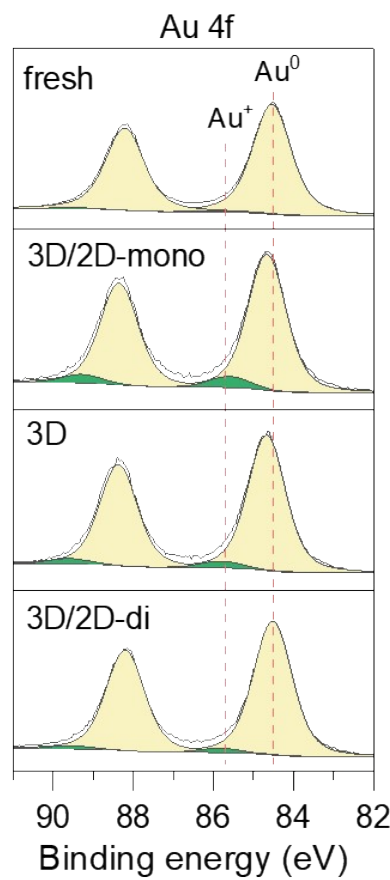


Figure S 18 XPS spectra of fresh device and aged 3D/2D-mono, 3D and 3D/2D-di devices at 85 °C 2-suns for 300 h.

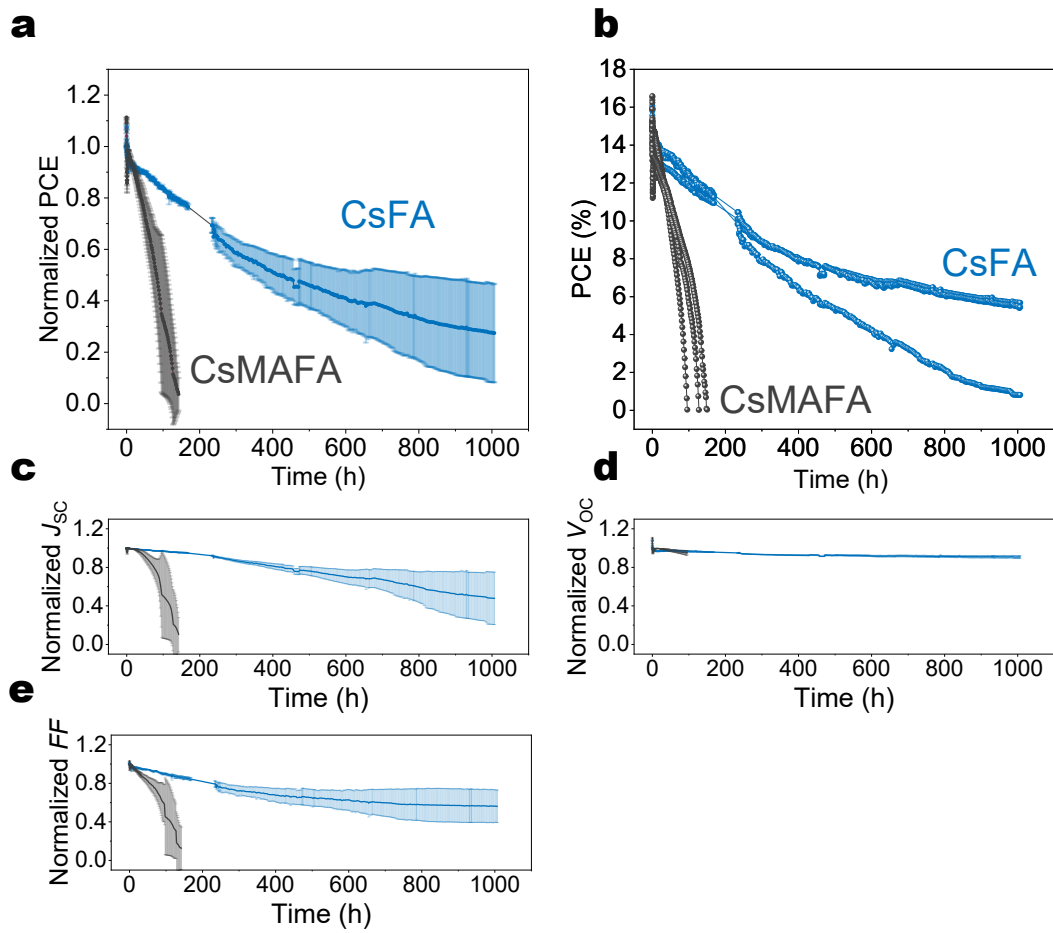


Figure S 19 Operational stability performance of CsMAFA and CsFA devices under 85°C and 2-suns illumination: (a-e) Normalized PCE, unnormalized PCE, J_{SC} , V_{OC} , and FF. Error bar represents the standard deviation of three individual devices. Each color contains 3 samples in Figure S 19b. As there is a fast burn-in at the very beginning due to the negative temperature coefficient, data were normalized at 0.6 h when the chamber's temperature increased to 80-85°C

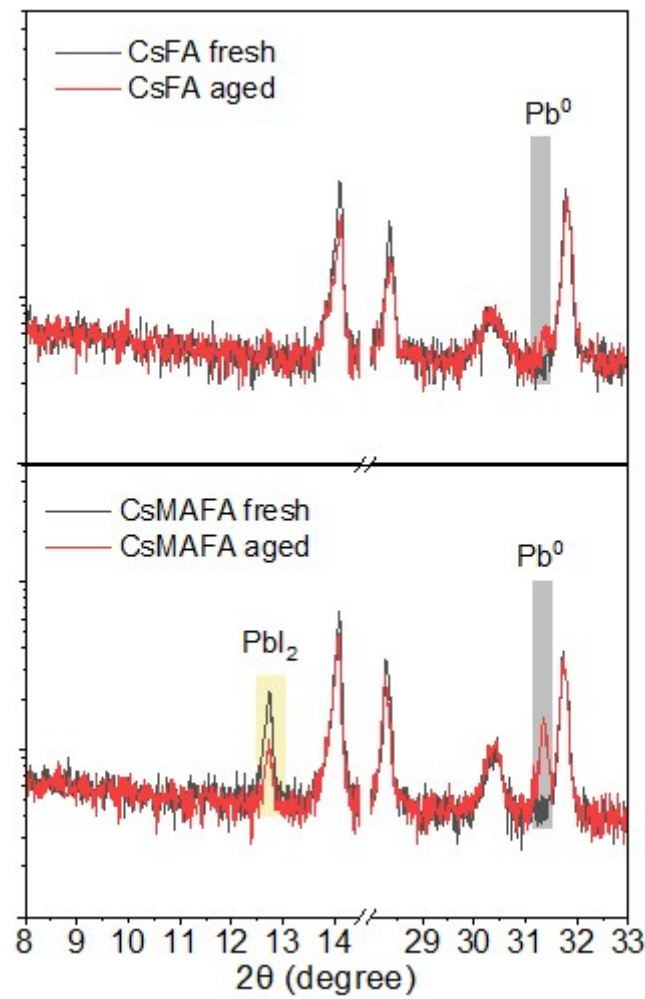


Figure S 20 XRD pattern of the CsMAFA and CsFA devices before and after ageing under 85°C 2-suns for 100 hours.

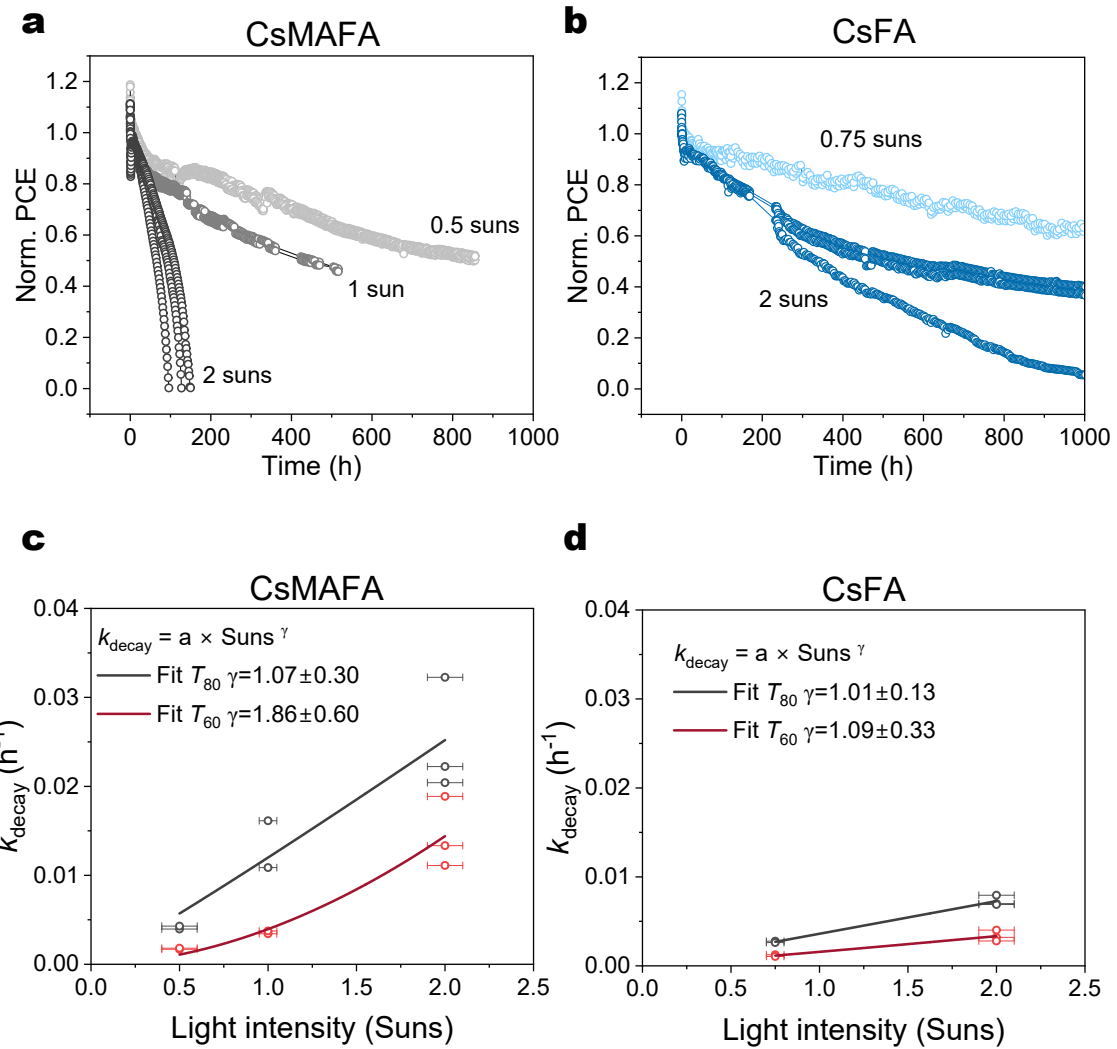


Figure S 21 (a-b) CsMAFA and CsFA based devices stability under different light intensities. As there is a fast burn-in at the very beginning due to the negative temperature coefficient, data were normalized at 0.6 h when the chamber's temperature increased to 80-85°C. (c-d) Fitting the acceleration factor of light using $k_{decay} = a \times \text{Suns}^{\gamma}$, where a is constant, γ is the acceleration factor and $k_{decay} = 1/T_{80}$ or $1/T_{60}$.

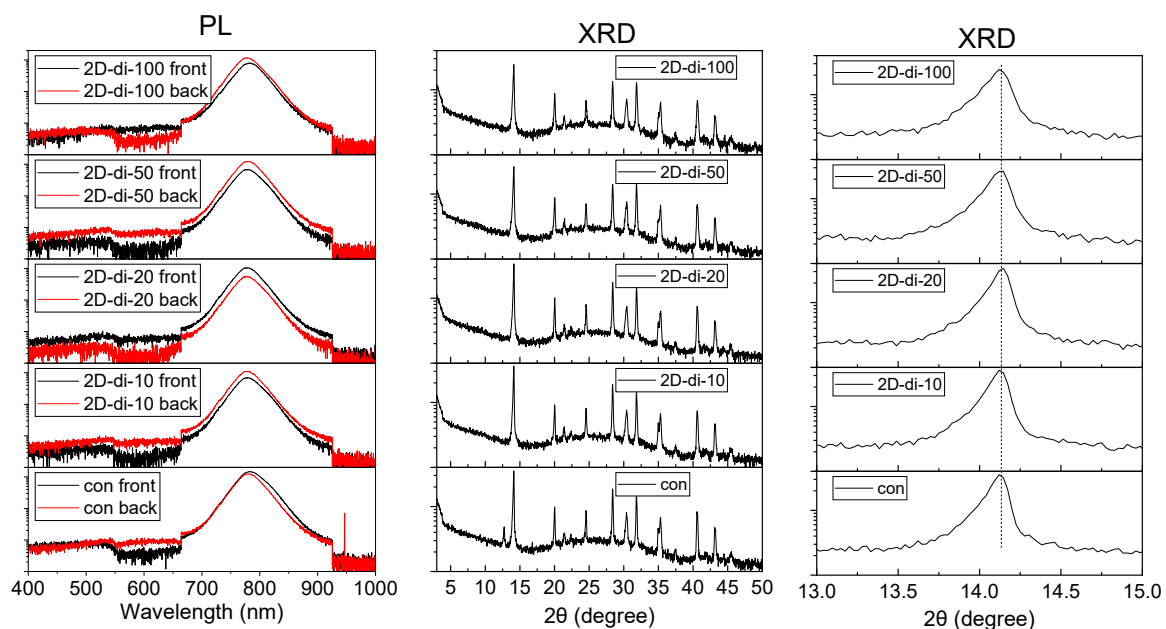
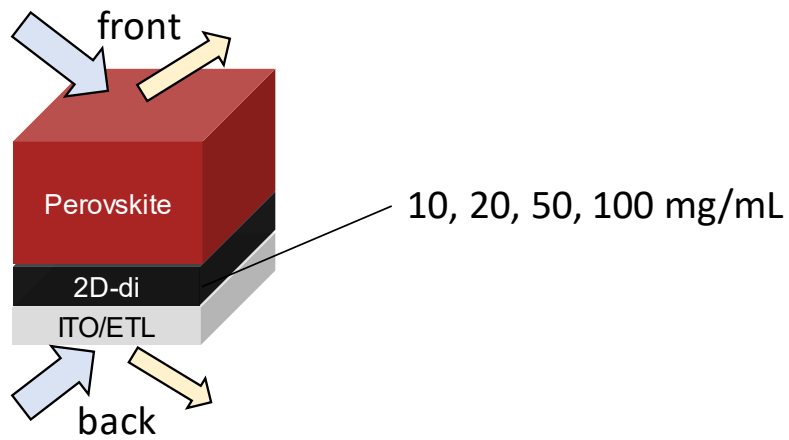


Figure S 22 The PL spectra and XRD patterns of perovskite films treated by di-ammonium ligand with different concentrations (10, 20, 50, 100 mg/mL in DMF). 10 mg/mL is the optimized concentration used in operational stability testing. The wavelength of excitation light is 375 nm. There is no 2D PL peak at short wavelength region and no 2D characteristic XRD peak at around 8° . The position of (100) XRD diffraction peak does not change when different concentrations of di-ammonium ligand are introduced.

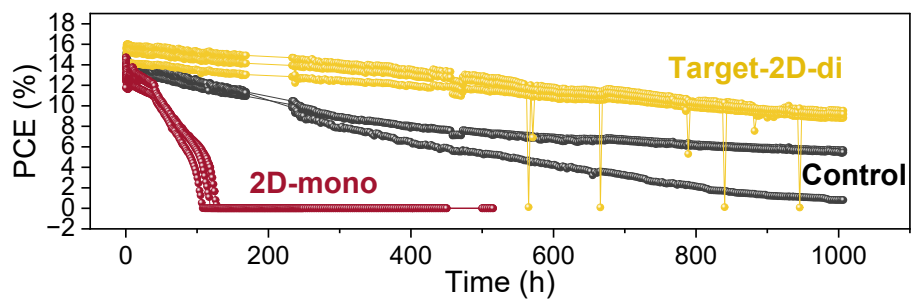


Figure S 23 The unnormalized PCE of devices based on control, 2D-mono and target-2D-di. Each color contains three independent devices.

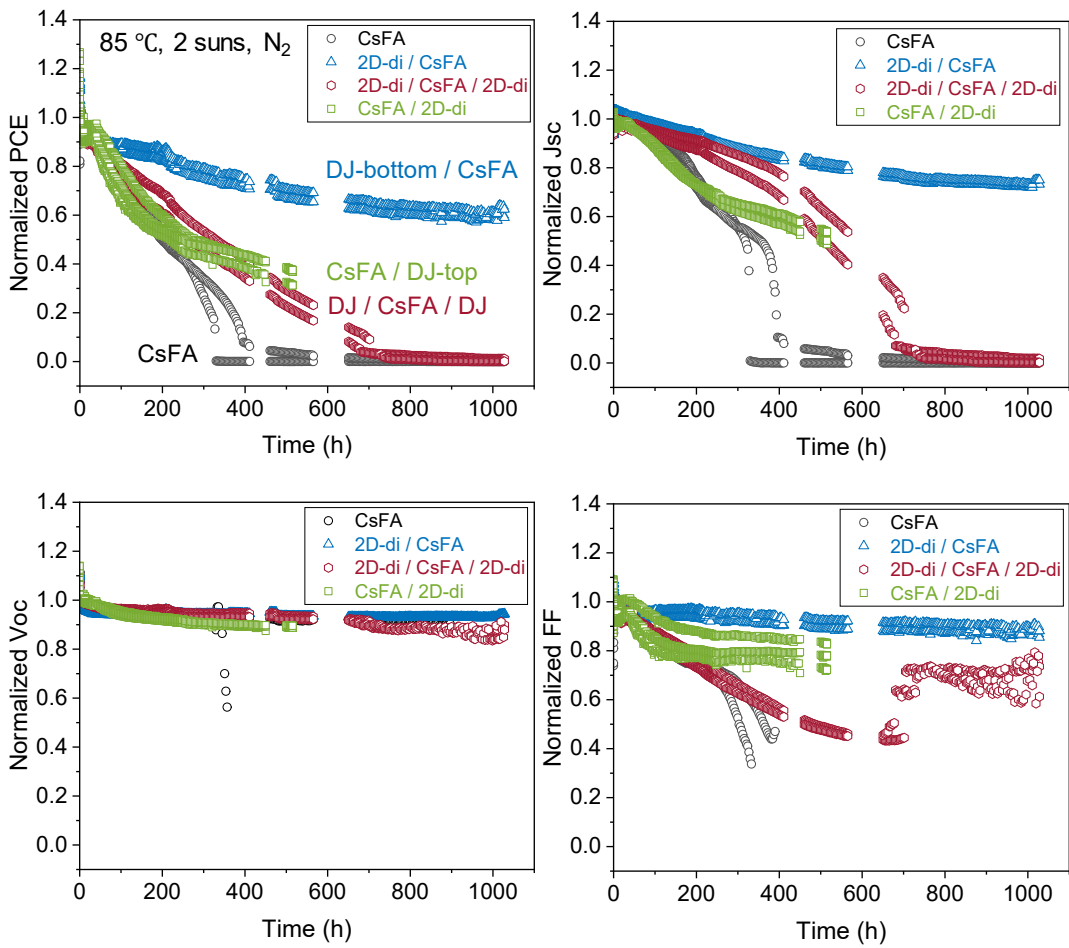


Figure S 24 Operational stability under 85°C and 2-suns illumination. Di-ammonium ligand (BAI_2) was introduced at bottom interface (2D-di/CsFA), at top interface (CsFA/2D-di) or at both interfaces (2D-di /CsFA/2D-di). The bottom treated devices (2D-di /CsFA) show the best stability, while the unpassivated devices (CsFA) are the worst. The 2D-di-top treatment inducing iodide interstitial near top interface is not beneficial to the stability. As there is a fast burn-in at the very beginning due to the negative temperature coefficient, data were normalized at 0.6 h when the chamber's temperature increased to 80-85°C

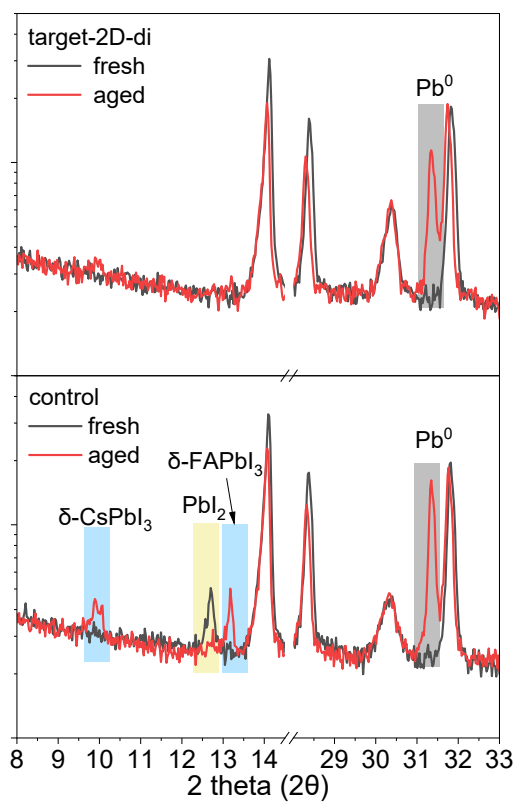


Figure S 25 XRD pattern of the control (CsFA-based) and target-2D-di (CsFA with 2D-di bottom) devices before and after ageing under 85°C 2-suns for 300 hours.

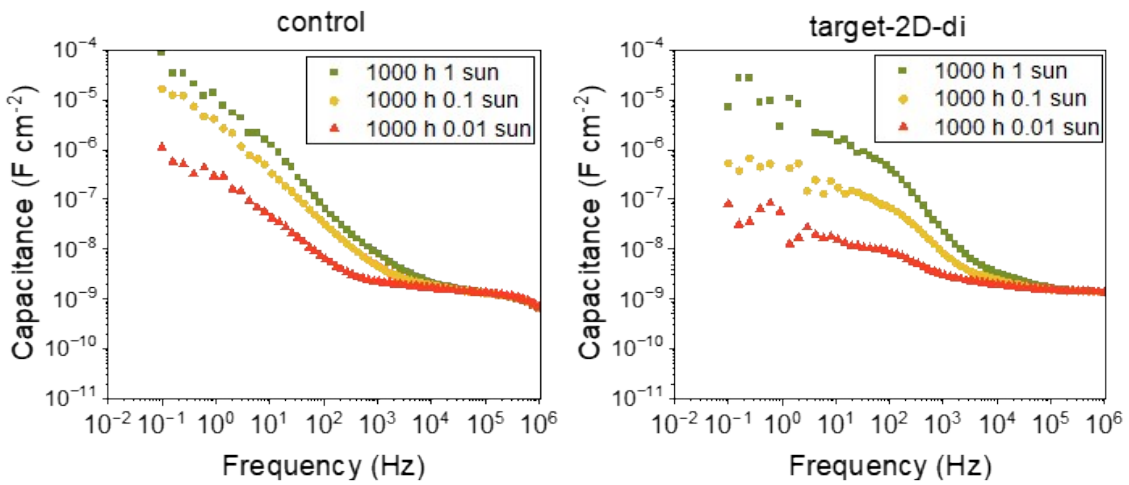


Figure S 26 Capacitance versus frequency plot of control and target-2D-di samples after 85 °C 2-suns degradation. The impedance was carried out at short-circuit and different illumination intensities. It shows that the target-2D-di device has around one order of magnitude lower response at low frequency than the untreated device, indicating suppressed recombination (caused by traps)¹³.

Table S 2 Summary of operational stability under harsh conditions (>80 °C)

Device structure	Temperature Light intensity	PCE remain	Ref.
p-i-n FTO/NiO_x/AlO_x/ Cs_{0.05}MA_{0.16}FA_{0.79}PbI₃ /C₆₀/BCP/Cu	85°C, 1-sun	2000 h (100%)	¹⁴
p-i-n FTO/2PACz/ Cs_{0.05}MA_{0.05}FA_{0.9}PbI₃ /345FAn/C₆₀/SnO₂/Ag	85°C, 0.8-sun	1586 h (84%)	¹⁵
p-i-n ITO/PTAA/ Cs_{0.10}FA_{0.90}PbI₃ + PEAMAI /C₆₀/BCP/Ag	85°C, 1-sun	1500 h (90%)	¹²
p-i-n ITO/PTAA-AlCl₄/ (CsPbI₃)_{0.05}[(FAPbI₃)_{0.92}(MAPbBr₃)_{0.08}]_{0.9} /PCBM/BCP/Ag	85 °C, 1-sun	1500 h (93%)	¹⁶
p-i-n FTO/NiOx/MeO-4PACz/DPPP/ Cs_{0.05}FA_{0.95}PbI₃ PEAI/C₆₀/BCP/Cr/Cu	85°C, 0.9-sun	1500 h (108%)	¹⁷
p-i-n ITO/NiO_x/MeO-4PADBC/ Cs_{0.05}MA_{0.1}FA_{0.85}PbI₃ /C₆₀/BCP/Ag	85°C, 1-sun	1200 h (74%)	¹⁸
p-i-n ITO/PTAA/ Cs_{0.07}FA_{0.93}PbI₃ BiOBr/C₆₀/BCP/Ag	85°C, 1-sun	1000 h (91%)	¹⁹
p-i-n ITO/mix-SAM/ Rb_{0.05}Cs_{0.05}MA_{0.05}FA_{0.85}Pb_{2.85}Br_{0.15} /C₆₀/SnO₂/Ag or Au	85°C, 1.2-sun	1000 h (80%) (extrapolated)	²⁰
p-i-n ITO/PTAA/ Cs_{0.05}(MA_{0.15}FA_{0.85})_{0.95}Pb(I_{0.85}Br_{0.15})₃ /PCBM/ZrL3: bis C₆₀/Ag	85°C, 1-sun	1000 h (92%)	²¹
p-i-n ITO/SAM/ Cs_{0.2}FA_{0.80}PbI₃ C[4]P/PCBM/C₆₀/BCF/Ag	85°C, 1-sun	500 h (87%)	²²

p-i-n				
FTO/MeO-2PACz/ Rb_{0.05}Cs_{0.05}MA_{0.05}FA_{0.85}Pb_{2.85}Br_{0.15} /C₆₀/YbO_x/Cu	85°C, 1-sun	500 h (85%)		²³
p-i-n				
ITO/MeO-2PACz/ FAPbI₃-2D /C₆₀/BCP/Cu	85°C, 1-sun	1000 h (97%)		²⁴
p-i-n				
ITO/DC-TMPS/ Cs_{0.05}(FA_{0.95}MA_{0.05})_{0.95}Pb(I_{0.95}Br_{0.05})₃ /C₆₀/ZnO/Au	85°C, 1-sun	1200 h (98%)		²⁵
ITO/2PACz/ FA_{0.92}Cs_{0.08}PbI₃/HUBLA /C60/BCP/Au	85°C, 1-sun	1500h 94%		²⁶
n-i-p				
FTO/TiO₂/Al₂O₃/ CsPbI₃ /Cs₂PbI₂Cl₂/CuSCN/Cr/Au	85°C & 110°C 1.2-sun	85°C 4000h (85%) 110°C 2300h (80%)		²⁷
n-i-p				
ITO/SnO₂-CBD/SnO₂-np/ MAFAPbIBr /PTAA-HFDF/MoO_x/Au	85°C, 1-sun	1000 h (92%)		²⁸
n-i-p				
ITO/SnO₂-CBD/ Cs_{0.05}MA_{0.05}FA_{0.9}PbI₃ /PTAA/Au	85°C, 1-sun	1250 h (85%)		²⁹
n-i-p				
ITO/SnO₂/ CsMAFAGAPbIBr /L3/MoO_x/Au	85°C, 1-sun	500 h (85%)		³⁰
n-i-p				
ITO/SnO₂-CBD/ Cs_{0.1}FA_{0.9}PbI₃ + selenophene /OAI/Spiro-PTAA/Au	85°C, 1-sun	500 h (89%)		³¹
n-i-p				
ITO/SnO₂/PCBM/ Cs_{0.15}FA_{0.85}PbI_{2.75}Br_{0.25} /PDCBT/PTAA/Au	85°C, 2-suns	560 h (80%)		This work

Table S 3 The parameters for $J-V$ curves simulation

Parameter	Symbol	3D 0.6 h	3D/2D-mono 0.6 h	3D/2D-di 0.6 h	Unit
Temperature	T		360		K
Thickness of perovskite	d_{pero}		500		nm
Thickness of ETL (SnO_2)	d_{ETL}		20		nm
Thickness of HTL (PTAA)	d_{HTL}		50		nm
Electron mobility in perovskite	$\mu_{\text{pero,n}}$		6×10^{-4}		m^2/Vs
Hole mobility in perovskite	$\mu_{\text{pero,p}}$		8×10^{-4}		m^2/Vs
Electron mobility in ETL	μ_{ETL}		1×10^{-4}		m^2/Vs
Hole mobility in HTL	μ_{HTL}		5×10^{-8}		m^2/Vs
Density of state in perovskite	$N_{\text{C/V,pero}}$		3.1×10^{24}		m^{-3}
Density of state in ETL	$N_{\text{C/V,ETL}}$		2.7×10^{24}		m^{-3}
Density of state in HTL	$N_{\text{C/V,HTL}}$		5×10^{25}		m^{-3}
Doping concentration in ETL	$N_{\text{e,ETL}}$		0		m^{-3}
Doping concentration in HTL	$N_{\text{h,HTL}}$		5×10^{23}		m^{-3}
Conduction band of perovskite	$E_{\text{C,pero}}$		3.8		eV
Valance band of perovskite	$E_{\text{V,pero}}$		5.4		eV
Conduction band of ETL	$E_{\text{C,ETL}}$		3.9		eV
Valance band of ETL	$E_{\text{V,ETL}}$		7.9		eV
Conduction band of HTL	$E_{\text{C,HTL}}$		2.25		eV
Valance band of HTL	$E_{\text{V,HTL}}$		5.25		eV
Work function of cathode	W_{ITO}		4.0		eV
Work function of anode	W_{Au}		5.1		eV
Relative dielectric constant of perovskite	$\epsilon_{\text{r,pero}}$		24		
Relative dielectric constant of ETL	$\epsilon_{\text{r,ETL}}$		3		
Relative dielectric constant of HTL	$\epsilon_{\text{r,HTL}}$		3		
Capture coefficient for electrons	C_n		2×10^{-13}		m^3/s
Capture coefficient for holes	C_p		6.77×10^{-14}		m^3/s
Trap density in perovskite	$N_{\text{t,bulk}}$		2.2×10^{20}		m^{-3}
Interface trap density at ETL/Perovskite	$N_{\text{t,ETL}}$		5×10^{13}		m^{-2}
Interface trap density at HTL/Perovskite	$N_{\text{t,HTL}}$	6×10^{14}	1×10^{14}	1.5×10^{14}	m^{-2}
Energy level of all traps	E_{trap}		4.91		eV
Mobile negative ions concentration	N_{ion}	1.5×10^{22}	1.3×10^{22}	1.3×10^{22}	m^{-3}
Shunt resistance	R_{sh}		2000		$\Omega \text{ cm}^2$
Series resistance	R_s	1	2.5	2	$\Omega \text{ cm}^2$

Table S 4 The parameters for simulation showed in Figure 4 and Figure S 14.

hours \	R_s ($\Omega \text{ cm}^2$)	μ_{HTL} ($10^{-8} \text{ m}^2 \text{V}^{-1} \text{s}^{-1}$)	$N_{\text{h,HTL}}$ (10^{23} m^{-3})	$N_{\text{t,HTL}}$ (10^{14} m^{-2})	$N_{\text{t,bulk}}$ (10^{20} m^{-3})	N_{ion} (10^{22} m^{-3})
3D/2D-mono						
0.6	2.5	5	5	1	2.2	1.3
5	3.5	5	5	5	2.2	1.3
15	6	5	5	10	4	1.3
25	9	1	1	10	6	2
35	70	0.1	0.2	10	6	2
3D						
0.6	1	5	5	6	2.2	1.5
10	1.7	5	5	6	3.5	1.9
50	2	3	2	6	6	3
100	6	0.8	1	6	20	3
125	70	0.1	0.2	6	20	3
3D/2D-di						
0.6	2	5	5	1.5	2.2	1.3
25	2	5	5	1.5	2.2	1.8
75	2.5	5	5	4	22	2.2
150	3	1	1	4	40	2.2
200	3.5	0.7	0.7	4	45	2.3

References

1. Zhao, Y.; Heumueller, T.; Zhang, J.; Luo, J.; Kasian, O.; Langner, S.; Kupfer, C.; Liu, B.; Zhong, Y.; Elia, J.; Osvet, A.; Wu, J.; Liu, C.; Wan, Z.; Jia, C.; Li, N.; Hauch, J.; Brabec, C. J., *Nature Energy* 2021, **7** (2), 144-152.
2. Koopmans, M.; Corre, V.; Koster, L., *Journal of Open Source Software* 2022, **7** (70), 3727.
3. Li, X.; Hoffman, J. M.; Kanatzidis, M. G., *Chem Rev* 2021, **121** (4), 2230-2291.
4. Tremblay, M.-H.; Bacsa, J.; Zhao, B.; Pulvirenti, F.; Barlow, S.; Marder, S. R., *Chem. Mat.* 2019, **31** (16), 6145-6153.
5. Billing, D. G.; Lemmerer, A., *Acta Crystallogr B* 2007, **63** (Pt 5), 735-47.
6. Zhang, F.; Park, S. Y.; Yao, C.; Lu, H.; Dunfield, S. P.; Xiao, C.; Ulicna, S.; Zhao, X.; Du Hill, L.; Chen, X.; Wang, X.; Mundt, L. E.; Stone, K. H.; Schelhas, L. T.; Teeter, G.; Parkin, S.; Ratcliff, E. L.; Loo, Y. L.; Berry, J. J.; Beard, M. C.; Yan, Y.; Larson, B. W.; Zhu, K., *Science* 2022, **375** (6576), 71-76.
7. Ma, C.; Shen, D.; Huang, B.; Li, X.; Chen, W.-C.; Lo, M.-F.; Wang, P.; Hon-Wah Lam, M.; Lu, Y.; Ma, B.; Lee, C.-S., *Journal of Materials Chemistry A* 2019, **7** (15), 8811-8817.
8. Liu, Y.; Guo, J.; Zhou, H.; Li, C.; Guo, X., *J Am Chem Soc* 2024, **146** (12), 8198-8205.
9. Yu, T.; Zhang, L.; Shen, J.; Fu, Y.; Fu, Y., *Dalton Trans* 2014, **43** (34), 13115-21.
10. Safdari, M.; Svensson, P. H.; Hoang, M. T.; Oh, I.; Kloof, L.; Gardner, J. M., *Journal of Materials Chemistry A* 2016, **4** (40), 15638-15646.
11. Lemmerer, A.; Billing, D. G., *CrystEngComm* 2012, **14** (6).
12. Wang, M.; Shi, Z.; Fei, C.; Deng, Z. J. D.; Yang, G.; Dunfield, S. P.; Fenning, D. P.; Huang, J., *Nature Energy* 2023, **8** (11), 1229-1239.
13. Bennett, L. J.; Riquelme, A. J.; Anta, J. A.; Courtier, N. E.; Richardson, G., *Physical Review Applied* 2023, **19** (1).
14. Yang, Y.; Cheng, S.; Zhu, X.; Li, S.; Zheng, Z.; Zhao, K.; Ji, L.; Li, R.; Liu, Y.; Liu, C.; Lin, Q.; Yan, N.; Wang, Z., *Nature Energy* 2023, **9** (1), 37-46.
15. Park, S. M.; Wei, M.; Xu, J.; Atapattu, H. R.; Eickemeyer, F. T.; Darabi, K.; Grater, L.; Yang, Y.; Liu, C.; Teale, S.; Chen, B.; Chen, H.; Wang, T.; Zeng, L.; Maxwell, A.; Wang, Z.; Rao, K. R.; Cai, Z.; Zakeeruddin, S. M.; Pham, J. T.; Risko, C. M.; Amassian, A.; Kanatzidis, M. G.; Graham, K. R.; Gratzel, M.; Sargent, E. H., *Science* 2023, **381** (6654), 209-215.
16. Wang, T.; Qiao, L.; Ye, T. S.; Kong, W. Y.; Zeng, F.; Zhang, Y.; Sun, R. T.; Zhang, L.; Chen, H.; Zheng, R. K.; Yang, X. D., *Journal of Materials Chemistry A* 2022, **10** (35), 18014-18020.
17. Li, C.; Wang, X.; Bi, E.; Jiang, F.; Park, S. M.; Li, Y.; Chen, L.; Wang, Z.; Zeng, L.; Chen, H.; Liu, Y.; Grice, C. R.; Abudulimu, A.; Chung, J.; Xian, Y.; Zhu, T.; Lai, H.; Chen, B.; Ellingson, R. J.; Fu, F.; Ginger, D. S.; Song, Z.; Sargent, E. H.; Yan, Y., *Science* 2023, **379** (6633), 690-694.
18. Li, Z.; Sun, X.; Zheng, X.; Li, B.; Gao, D.; Zhang, S.; Wu, X.; Li, S.; Gong, J.; Luther, J. M.; Li, Z.; Zhu, Z., *Science* 2023, **382** (6668), 284-289.
19. Zhang, H.; Wang, F. L.; Li, B. X.; Sun, M.; Li, K.; Wang, H.; Jen, A. K. Y., *ACS Energy Lett.* 2023, **9** (1), 176-185.
20. Jiang, Q.; Tirawat, R.; Kerner, R. A.; Gaulding, E. A.; Xian, Y.; Wang, X.; Newkirk, J. M.; Yan, Y.; Berry, J. J.; Zhu, K., *Nature* 2023, **623** (7986), 313-318.
21. Wu, S.; Li, Z.; Li, M. Q.; Diao, Y.; Lin, F.; Liu, T.; Zhang, J.; Tieu, P.; Gao, W.; Qi, F.; Pan, X.; Xu, Z.; Zhu, Z.; Jen, A. K., *Nat Nanotechnol* 2020, **15** (11), 934-940.

22. Guo, H.; Wang, X.; Li, C.; Hu, H.; Zhang, H.; Zhang, L.; Zhu, W. H.; Wu, Y., *Adv Mater* 2023, **35** (26), e2301871.
23. Chen, P.; Xiao, Y.; Hu, J.; Li, S.; Luo, D.; Su, R.; Caprioglio, P.; Kaienburg, P.; Jia, X.; Chen, N.; Wu, J.; Sui, Y.; Tang, P.; Yan, H.; Huang, T.; Yu, M.; Li, Q.; Zhao, L.; Hou, C. H.; You, Y. W.; Shyue, J. J.; Wang, D.; Li, X.; Zhao, Q.; Gong, Q.; Lu, Z. H.; Snaith, H. J.; Zhu, R., *Nature* 2024, **625** (7995), 516-522.
24. Sidhik, S.; Metcalf, I.; Li, W.; Kodalle, T.; Dolan, C. J.; Khalili, M.; Hou, J.; Mandani, F.; Torma, A.; Zhang, H.; Garai, R.; Persaud, J.; Marciel, A.; Muro Puente, I. A.; Reddy, G. N. M.; Balvanz, A.; Alam, M. A.; Katan, C.; Tsai, E.; Ginger, D.; Fenning, D. P.; Kanatzidis, M. G.; Sutter-Fella, C. M.; Even, J.; Mohite, A. D., *Science* 2024, **384** (6701), 1227-1235.
25. Tang, H.; Shen, Z.; Shen, Y.; Yan, G.; Wang, Y.; Han, Q.; Han, L., *Science* 2024, **383** (6688), 1236-1240.
26. Wang, W. T.; Holzhey, P.; Zhou, N.; Zhang, Q.; Zhou, S.; Duijnstee, E. A.; Rietwyk, K. J.; Lin, J. Y.; Mu, Y.; Zhang, Y.; Bach, U.; Wu, C. G.; Yip, H. L.; Snaith, H. J.; Feng, S. P., *Nature* 2024, **632** (8024), 294-300.
27. Zhao, X.; Liu, T.; Burlingame, Q. C.; Liu, T.; Holley, R., 3rd; Cheng, G.; Yao, N.; Gao, F.; Loo, Y. L., *Science* 2022, **377** (6603), 307-310.
28. Wang, T.; Zhang, Y.; Kong, W.; Qiao, L.; Peng, B.; Shen, Z.; Han, Q.; Chen, H.; Yuan, Z.; Zheng, R.; Yang, X., *Science* 2022, **377** (6611), 1227-1232.
29. Liu, C.; Yang, Y.; Chen, H.; Spanopoulos, I.; Bati, A. S. R.; Gilley, I. W.; Chen, J.; Maxwell, A.; Vishal, B.; Reynolds, R. P.; Wiggins, T. E.; Wang, Z.; Huang, C.; Fletcher, J.; Liu, Y.; Chen, L. X.; De Wolf, S.; Chen, B.; Zheng, D.; Marks, T. J.; Facchetti, A.; Sargent, E. H.; Kanatzidis, M. G., *Nature* 2024, 10.1038/s41586-024-07764-8.
30. Yuan, L. G.; Zhu, W. Y.; Zhang, Y. H.; Li, Y.; Chan, C. C. S.; Qin, M. C.; Qiu, J. H.; Zhang, K. C.; Huang, J. X.; Wang, J. R.; Luo, H. M.; Zhang, Z.; Chen, R. P.; Liang, W. X.; Wei, Q.; Wong, K. S.; Lu, X. H.; Li, N.; Brabec, C. J.; Ding, L. M.; Yan, K. Y., *Energy & Environmental Science* 2023, **16** (4), 1597-1609.
31. Bai, Y.; Huang, Z.; Zhang, X.; Lu, J.; Niu, X.; He, Z.; Zhu, C.; Xiao, M.; Song, Q.; Wei, X.; Wang, C.; Cui, Z.; Dou, J.; Chen, Y.; Pei, F.; Zai, H.; Wang, W.; Song, T.; An, P.; Zhang, J.; Dong, J.; Li, Y.; Shi, J.; Jin, H.; Chen, P.; Sun, Y.; Li, Y.; Chen, H.; Wei, Z.; Zhou, H.; Chen, Q., *Science* 2022, **378** (6621), 747-754.